Soft and stretchable thienopyrroledione-based polymers via direct arylation

Angela Lin[a], Lorenzo Guio[b], Garrett LeCroy[c], Stanley Lo[a,d], Adnan Sharif[e], Yunfei Wang[f], Alberto Salleo[c], Xiaodan Gu[f], Christine K. Luscombe[b,g], Helen Tran[a,d,h]**

[a.] A. Lin, S. Lo, Prof. H. Tran
Department of Chemistry, University of Toronto,
80 St. George Street, Toronto, ON, M5S 3H6, Canada
*Email: tran@utoronto.ca

[b.] L. Guio, Prof. C.K. Luscombe
Department of Materials Science and Engineering, University of Washington
Seattle, Washington 98195, United States
*E-mail: christine.luscombe@oist.jp

[c.] Garrett LeCroy, Prof. A. Salleo
Department of Materials Science and Engineering, Stanford University
Stanford, CA 94305, USA

[d.] Stanley Lo
Vector Institute for Artificial Intelligence
661 University Ave. Suite 710, Toronto, ON M5G 1M1, Canada

[e.] A. Sharif, Prof. H. Tran
Department of Chemical Engineering, University of Toronto,
200 College St, Toronto, Toronto, ON, M5S 3E5, Canada

[f.] Y. Wang, Prof. X. Gu
School of Polymer Science and Engineering, The University of Southern Mississippi
Hattiesburg, MS 39406, USA

[g.] Prof. C.K. Luscombe
Okinawa Institute of Science and Technology Graduate University, pi-Conjugated Polymers Unit, Onna-son, Okinawa 904-0495, Japan

[h] Prof. H. Tran
Acceleration Consortium, University of Toronto,
80 St George St, Toronto, ON M5S 3H6, Canada

Keywords: direct arylation polymerization, semiconducting polymer, donor-acceptor, soft, stretchable

Abstract.

π-conjugated polymers (CPs) that are concurrently soft and stretchable are needed for deformable electronics. Molecular level modification of indacenodithiophene (IDT) copolymers, a class of CPs that exhibit high hole mobilities, is an approach that could help realize intrinsically soft and stretchable CPs. There are currently numerous examples of design strategies to adjust the stretchability of CPs, but imparting softness is comparatively less studied. In a previous study, poly(indacenodithiophene-thienopyrroledione) (p(IDT_{C16}-TPD_{C8})) exhibited a significantly lower elastic modulus (*E)* in the 10s of MPa range compared to CPs that are typically in the ~1-10 GPa range. However, p(IDT_{C16}-TPD_{C8}) exhibited poor stretchability (crack onset strain, *CoS* = 7 %) and low hole mobility (μ_{hole}), potentially due to its low molecular weight (11 $kgmol^{-1}$). In our study, a systematic molecular weight series was constructed on the promising candidate for soft CPs, p(IDT_{C16}-TPD_{C8}), by optimizing direct arylation polymerization conditions in hopes of improving stretchability and μ_{hole} without significantly impacting *E.* We found p(IDT_{C16}-TPD_{C8}) at a degree of polymerization (DP) of 32 showed high stretchability (*CoS* > 100%) without significantly altering softness (*E* = 32 MPa), which to the best of our knowledge outperforms previously reported stretchable and soft CPs. To further study how molecular level modifications impact bulk polymer properties, we also built a MW series of a new polymer, poly(indacenodithieno[3,2-b]thiophene-thienopyrroledione) (p($IDTT_{C16}$-TPD_{C8})), which extends the π-conjugation of the IDT unit. In contrast to expectation, IDTT copolymers did not result in a greater average μ_{hole} when comparing between p($IDTT_{C16}$-TPD_{C8}) and p(IDT_{C16}-TPD_{C8}) with similar MWs despite their higher crystallinity observed by GIWAXS.While these findings warrant further investigation, our study points towards unique charge transport properties of IDT-based polymers.

1. Introduction

Towards the development of deformable electronics, π-conjugated polymers (CPs) that are concurrently soft and stretchable have been investigated to improve biocompatibility and ensure precise measurement of biological signals.[1–3] There have been significant advances in imparting stretchability in semiconducting CPs, where processing strategies [4,5] or molecular design[6–8] may lead to films that can maintain electronic performance with >100% strain. However, there have been relatively less literature examples of imparting low stiffness to semiconducting CPs.[9] While CPs inherently show lower elastic moduli (*E*, ~1-10 GPa) than inorganic counterparts (~100 GPa), the *E* of CPs are typically still orders of magnitude above the low moduli of biological tissue (Pa to low MPa range).[10] Matching a material's *E* with that of biological tissues has been shown to attenuate inflammatory immunological responses and lead to improved biocompatibility and long-term performance[11,12] A notable class of semiconducting CPs that can possess lower *E* are indacenodithiophene-co-benzothiadiazole (IDT-BT) donor-acceptor (D-A) copolymers. For example, Geng, Y. and coworkers reported p(IDT_{C16}-BT) having an *E* of 208.7 MPa with a molecular weight (MW) of 49 $kgmol^{-1}$. [13] Similarly, Luscombe, C.K. and coworkers reported-indacenodithiophene-co-thienopyrroledione (p(IDT_{C16}-TPD_{C1})) having an *E* from 110 to 410 MPa with a MW of 14 $kgmol^{-1}$.[14] Further building off this work, Luscombe, C.K. and coworkers showed that side chain substitution of the acceptor unit methyl (TPD_{C1}) to a linear octyl alkyl chain (TPD_{C8}), yielded a polymer p(IDT_{C16}-TPD_{C8}) having an *E* of 14 MPa with MW of 11 kg mol^{-1}.[15] p(IDT_{C16}-TPD_{C8}) represents one of the first semiconducting CPs with a *E* in the 10s of MPa range.[15] In these comparisons, it is important to note the *E* values were measured using different techniques (i.e., film-on-water, film-on-elastomer), which can lead to vastly different values. This necessitates the selection and inclusion of an appropriate reference CP that is well established as well as standard characterization protocols when exploring the polymer design space to allow for direct comparison. Additionally, while all the aforementioned work

contributes towards the development of semiconducting CPs with improved moduli matching (i.e., lower stiffness) with biological tissue, the stretchability of these CPs remains low (i.e. p(IDT_{C16}-BT) [13] has a crack onset strain (*CoS*) of 9.2 %, p(IDT_{C16}-TPD_{C1}) [14] has a *CoS* of 3%, and p(IDT_{C16}-TPD_{C8}) has a *CoS* of 7 %). [15]

A strategy to increase the stretchability of semiconducting CPs is to increase the MW as the strain would be loaded through chain entanglement rather than forming cracks.[13,16,17] The entanglement of chains at higher MW can also lower the crystallinity of the CPs, creating amorphous regions to load external strain.[13,17] The impact of MW on semiconducting CPs has been well studied in P3HT[16,18] and p(IDT_{C16}-BT)[13,19], where increasing MW tends to increase *E*. For example, for p(IDT_{C16}-BT), *E* of 208.7 MPa was measured for 49 $kgmol^{-1}$ and *E* of 1007.1 MPa was measured for 1049.6 $kgmol^{-1}$.*[13]* As the TPD copolymers exhibit substantially lower *E* (14 MPa) at low MW (M_n = 11 $kgmol^{-1}$), it is worthwhile to investigate increasing MW and measuring the impact on *E*, *CoS,* and μ_{avg}. The MW of previous TPD copolymers were limited to low MWs as the authors were primarily interested in the impact of sidechain on TPD copolymers.[15] Furthermore, the polymers were synthesized via direct arylation polymerization (DArP), which is a C-H activation polymerization method that requires reaction optimization to achieve higher MW and defect-free polymers.[15]

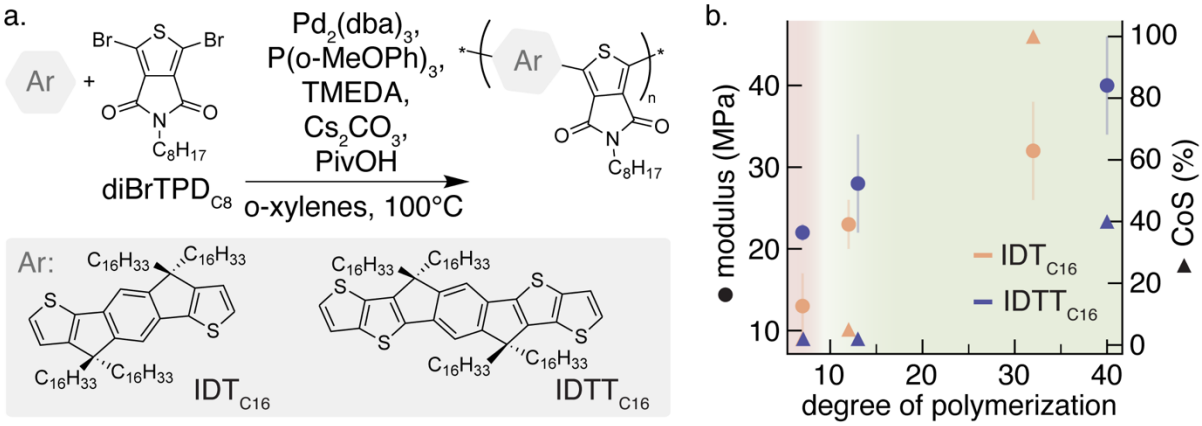

Figure 1. a) General direct arylation polymerization conditions for synthesizing the different MW TPD-based IDT and IDTT copolymer series. b) Summarized elastic moduli and *CoS* measurement results for the MW weight range in this study, with a red highlight over the DP

range achieved in a previous study [15] and a green highlight over the DP range achieved in this study.

In this report, p(IDT_{C16}-TPD_{C8}) with varied number-average MWs (M_n from 10 to 46 $kgmol^{-1}$) was synthesized via DArP (Figure 1a), achieving higher MWs than previously reported.[15] A discussion of the different DArP conditions tested and the selection of reagents used in this study is included to provide insight into polymerization optimization. The range of M_n facilitates systematic investigation of MW-dependent behaviors of electrical (e.g., field effect mobility, μ_{avg}) and mechanical (e.g., *CoS*, *E*) metrics of interest. We demonstrate that p(IDT_{C16}-TPD_{C8}) with M_n of 46 $kgmol^{-1}$ achieved an impressive *CoS* value >100%, low *E* of 32 MPa, and the highest hole mobility of the TPD-based copolymers in this study (0.0074 $cm^2V^{-1}s^{-1}$), outperforming previously demonstrated TPD-based copolymers (Figure 1b).

We also report the first copolymerization of an extended fused ring donor unit, indacenodithieno[3,2-b]thiophene ($IDTT_{C16}$), with TPD_{C8} to prepare varied MW p($IDTT_{C16}$-TPD_{C8}) (M_n from 11 to 62 $kgmol^{-1}$) as a potential strategy to improve the μ_{avg} of p(IDT_{C16}-TPD_{C8}). Extending the conjugation length of the donor unit by adding additional thiophene rings to IDT has been previously demonstrated with p($IDTT_{C16}$-BT) to exhibit saturation hole mobility up to 6.6 $cm^2V^{-1}s^{-1}$. [20] This is potentially due to the reduction in energetic disorder and extending of the π-conjugation of the polymer backbone for intramolecular charge transport.[20] However, this study did not compare directly to a reference p(IDT_{C16}-BT) device prepared in the same manner as their devices but was compared to a literature value of 3.6 $cm^2V^{-1}s^{-1}$ for p(IDT_{C16}-BT); thus, it is inconclusive if the extended core did truly exhibit improved electrical performance. Another study by McCulloch, I. and coworkers prepared devices with extended conjugated versions of IDT copolymerized with BT and found the average hole mobility of p($IDTT_{C16}$-BT) to be marginally lower than their reference p(IDT_{C16}-BT).[21] The Đ of their p($IDTT_{C16}$-BT) was larger than the other extended IDT polymers in their study (e.g., 2.6 for p($IDTT_{C16}$-BT) and 1.5 for dithiopheneindenofluorene(TIF)-*co*-BT)

which may have contributed to the observed polymer properties.[21] In our study, Đ between the IDT- and IDTT- TPD copolymer counterparts were carefully controlled to be similar with another. We observed that p($IDTT_{C16}$-TPD_{C8}) exhibited a higher degree of crystallinity but lower μ_{avg} compared to p(IDT_{C16}-TPD_{C8}), as measured with grazing-incidence wide-angle X-ray scattering (GIWAXS) and organic field effect transistors, respectively. This finding contributes to existing literature that the previous understanding of higher crystallinity being a necessity for achieving higher mobility is not always correct and motivates further detailed investigation on the morphology of these TPD-based copolymers.[22]

2. Results and Discussion

2.1. Polymer synthesis

A series of IDT_{C16}-TPD_{C8} (Figure 2a) and $IDTT_{C16}$-TPD_{C8} (Figure 2b) polymers with differing degree of polymerizations (DP) were synthesized by DArP to explore the effect of MW on polymer properties. Three DP ranges were prepared, denoted as low (DP 7), medium (DP ~12), and high (DP >32) MW (Figure 2a). DP will be primarily used in the rest of this study to describe the size of each polymer as the difference in the mass of the donor-acceptor units (e.g., 1425.5gmol^{-1} for IDT_{C16}-TPD_{C8} and 1537.6gmol^{-1} for $IDTT_{C16}$-TPD_{C8}) impacts clear comparison when using MW. [12,13,19] Detailed synthetic protocols and characterization of the polymer and monomers can be found the Supporting Information (SI) with a general polymerization procedure in the Experimental Methods below. The donor monomers (IDT_{C16} and $IDTT_{C16}$) are commercially available from Derthon and the acceptor monomer (TPD_{C8}) was synthesized as previously reported.[14,15,23] To achieve higher DP polymers for p(IDT_{C16}-TPD_{C8}), previously reported procedures[15,24] were used as a starting point for polymerization optimization. Factors such as monomer reactivity and solubility impact the ability to directly translate procedures between D-A polymers. Using our previous procedure for p(IDT_{C16}-TPD_{C8}), we could only achieve low DP (8, M_n ~11 kgmol^{-1}) and yields of ~50%. Varying reaction parameters (e.g., increasing concentration, reaction time, anhydrous solvent) did not

show any appreciable improvement in MW (Table S1). Generally, we did find that anhydrous solvent and increased concentration tend to increase yield (Table S1). However, increasing DP needed further exploration of conditions.

The addition of tetramethyethylene-diamine (TMEDA) as a co-ligand in DArP conditions has been previously found to help prevent structural defects, shorten reaction times and achieve higher DP and yield.[25] TMEDA inhibits the reduction of the monomers, which prevents undesirable side reactions (i.e., termination leading to low MW, homocoupling and branching defects) from occurring. Additionally, it has been established that there is a balance between using a high concentration to achieve higher MW and yield while having sufficient solvent to fully solubilize all reagents.[19] With these considerations in mind, we added TMEDA to our previous DArP conditions and varied the polymerization concentration (0.05 M to 0.4 M, IDT to solvent) to see the impact on DP, yield and structural integrity. Detailed findings for DP and yield are summarized in Table S2. Notably, we found that both high concentration (0.4M) and 10 mol % TMEDA was needed to achieve reproducible and high DP p(IDT_{C16}-TPD_{C8}), with a 4-fold increase in M_n from our initial procedure with 11 $kgmol^{-1}$ to 46 $kgmol^{-1}$(Table S2).

To construct the MW series, we varied stoichiometric monomer ratios in the optimized procedure used to synthesize high MW p(IDT_{C16}-TPD_{C8})-DP32 (46 $kgmol^{-1}$; 94% yield, 1 mol TPD:1 mol IDT) to prepare the medium MW p(IDT_{C16}-TPD_{C8})-DP12 (16 $kgmol^{-1}$; 1.04 mol TPD:1 mol IDT) and low MW p(IDT_{C16}-TPD_{C8}[22,23])-DP12 (10 $kgmol^{-1}$; 1.07 mol TPD:1 mol IDT). Approaches to achieve controlled DP typically use fractionation of synthesized polymers by recycling gel permeation chromatography (GPC) or Soxhlet extraction, which results in yield loss.[26,27] Controlling DP by systematically varying the stoichiometric ratios based on the Carothers equation (Equation S1) has been established in literature. [26,27] However, the Carothers equation assumes the extent of reaction is unity or close to unity and requires high purity for the Pd catalyst, which may cause discrepancies between calculated

and experimental results. [26,27] We found using the Carothers equation (Equation S1) provided a good starting point for finding suitable stoichiometric ratios, but experimental trial and error was needed to achieve a target DP due to slight experimental variations that can occur (i.e., temperature fluctuations, Pd catalyst purity, etc).

For the synthesis of p(IDTT$_{C16}$-TPD$_{C8}$), reaching unity for reaction extent was difficult and so to achieve similar DP and Đ ranges as the p(IDT$_{C16}$-TPD$_{C8}$) MW series, we varied reaction times, concentrations, and fractionated synthesized polymers using recycling GPC. We hypothesize that the difference between the IDT and IDTT polymers are due to differences in monomer reactivity between IDT and IDTT and the sensitivity of the approach to small variations in reagents used (i.e., Pd cat. purity). For p(IDTT$_{C16}$-TPD$_{C8}$), we observed the highest yield (80 %) with TMEDA and high concentration (Table S3). However, insoluble solids were observed if the reaction time was the same as what was done for p(IDT$_{C16}$-TPD$_{C8}$), likely due to the poor solubility of the growing p(IDTT$_{C16}$-TPD$_{C8}$) chains. When TMEDA was not added, insoluble solids were also observed (Entry 3, Table S5). This is potentially due to homocoupling and branching defects, which supports the need for TMEDA in preparing well-defined CPs via DArP.

The M_n of these polymers was characterized by high temperature GPC (HT-GPC) and the structural integrity by ^{1}H NMR spectroscopy (Figure 2). By ^{1}H NMR, the potential end groups and/or defects are labeled +. The spectrum of p(IDT$_{C16}$-TPD$_{C8}$)-DP7 and p(IDTT$_{C16}$-TPD$_{C8}$)-DP7 show more defined peaks compared to the medium and high polymers. This observation aligns with assigning the peaks to end groups as the peaks corresponding to end groups would relatively decrease in intensity as the polymer is higher in MW. However, as the peaks overlap with the main aromatic peaks for the polymers, comparison of relative integrations for peaks (aromatic to potential end group) is difficult, which makes definitive assignment not possible.

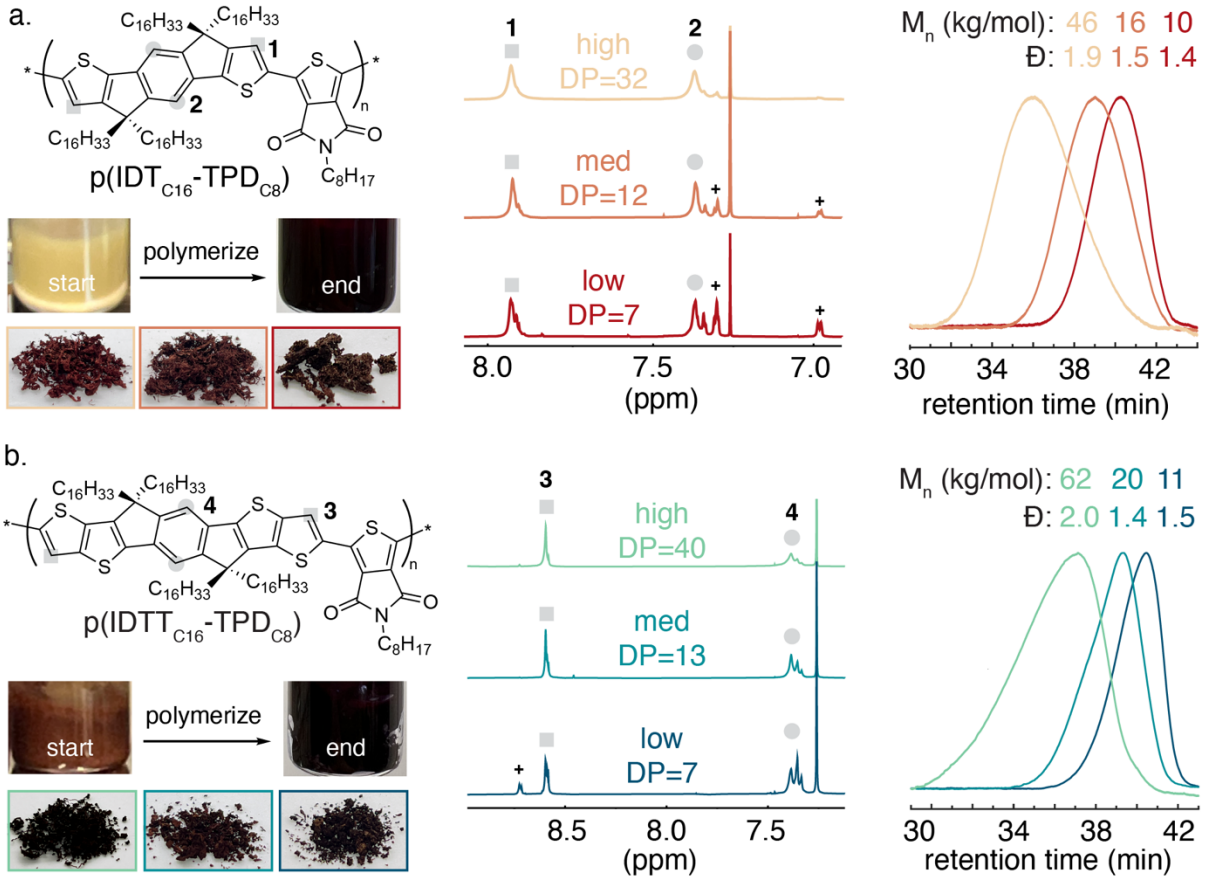

Figure 2. Synthesis of a molecular weight series for a) p(IDT$_{C16}$-TPD$_{C8}$) and b) p(IDTT$_{C16}$-TPD$_{C8}$), which was characterized for structure by proton NMR spectroscopy and molecular weight by GPC. Potential end group and/or defects labeled with +.

2.2. Mechanical characterization

Table 1. Summary of polymer properties for p(IDT$_{C16}$-TPD $_{C8}$) and p(IDTT$_{C16}$-TPD$_{C8}$)

Polymer	M_n (kg/mol)[a)]	Đ [a)]	DP [a)]	*E* (MPa)[b)]	*CoS* (%)[c)]
p(IDT$_{C16}$-BT)	55	2.0	42	140 ± 17	*ca.* 60
p(IDT$_{C16}$-TPD $_{C8}$)	10	1.4	7	13 ± 4	*ca.* 2
	16	1.5	12	23 ± 3	*ca.* 5
	46	1.9	32	32 ± 6	>100
p(IDTT$_{C16}$-TPD$_{C8}$)	11	1.5	7	22 ± 1	*ca.* 2
	20	1.4	13	28 ± 6	*ca.* 2
	62	2.0	40	40 ± 6	*ca.* 40

[a)]Number average molecular weight (M_n), dispersity (Đ), and degree of polymerization (DP) were measured by high-temperature gel permeation chromatography at 135 °C with a 0.5 mL/min flow rate. [b)]Average elastic modulus (*E*) and [c)]crack onset strain (*CoS*) of polymer thin films were measured by film-on-elastomer experiments as detailed in the SI.

Film-on-elastomer (FOE) thin film tensile measurements (Figure 4a) were performed to compare the mechanical properties of IDT and IDTT copolymers, with well-studied p(IDT_{C16}-BT)[13,19,21] serving as the reference. The mechanical metrics of interest, *E* and *CoS*, are tabulated in Table 1. Measuring *E* via mechanical buckling is an established method for thin film systems that may be difficult to measure with other methods.[28–33] For example, while film-on-water measurements avoid potential substrate effects, thin film breakage was observed with the low MW polymers when transferring to water (Figure S7), preventing a comparative study to higher MW polymers. Therefore, FOE was selected as it could capture *CoS* and *E* across the MW range in this study. As MW increases for the IDT-TPD series, *E* increases from 13 MPa for p(IDT_{C16}-TPD $_{C8}$)-DP7, 23 MPa for p(IDT_{C16}-TPD $_{C8}$)-DP12, to 32 MPa for p(IDT_{C16}-TPD $_{C8}$)-DP32. This trend was also observed for the IDTT-TPD series where *E* increases from 22 MPa for p($IDTT_{C16}$-TPD $_{C8}$)-DP7, 28 MPa for p($IDTT_{C16}$-TPD $_{C8}$)-DP13, to 40 MPa for p($IDTT_{C16}$-TPD $_{C8}$)-DP40. Detailed description for the FOE buckling method can be found in the Experimental Methods below and optical microscopy images of buckles in the SI (Figure S6). The slightly higher *E* for the IDTT-TPD series comparatively to the IDT-TPD series is attributed to the extended rigid aromatic donor unit imparting increased stiffness. The reference p(IDT_{C16}-BT)-DP42 has a *E* of 140 MPa, which is higher in *E* when compared to both IDTT-TPD and IDT-TPD copolymers at similar MW, indicating the acceptor unit modification was successful in lowering *E* for both copolymer series.

CoS measurements in the FOE method are used to determine the strain at which the material begins to show cracks by optical microscopy and p(IDT_{C16}-BT) has previously demonstrated high stretchability (*CoS* > 100 %) at a sufficiently high MW.[13] In this study,

p(IDT$_{C16}$-BT)-DP42 was synthesized to match the high MW regime TPD-based copolymers. The *CoS* of p(IDT$_{C16}$-BT)-DP42 was measured to be ca. 60% (Figure 4b). For p(IDTT$_{C16}$-TPD$_{C8}$), the low and medium DP polymers all cracked at relatively low strains (ca. 2 %) except for the high DP p(IDTT$_{C16}$-TPD$_{C8}$)-DP40 with a *CoS* of ca. 40% (Figure 4c). This observation aligns with what has been previously established for semiconducting polymers where increasing molecular weight tends to increase the density of entanglements, resulting in a material with a higher *CoS*.[13,16] The lower *CoS* measured for p(IDTT$_{C16}$-TPD$_{C8}$)-DP40 compared to p(IDT$_{C16}$-BT)-DP42 could be ascribed to its lower DP and/or increased crystallinity due to the extended donor unit. However, for p(IDT$_{C16}$-TPD$_{C8}$), significantly improved *CoS* was observed going from low to high DP where no cracks were observable even at 100 % strain for p(IDT$_{C16}$-TPD$_{C8}$)-DP32 (Figure 4c). This increase in *CoS* for p(IDT$_{C16}$-TPD$_{C8}$)-DP32, even when it is at a lower DP than p(IDT$_{C16}$-BT)-DP42, can be attributed primarily to the acceptor unit modification (i.e., BT to TPD$_{C8}$). This improvement in deformability appears to require a certain MW threshold to be hit first before *CoS* increases, but we find the MW to be lower for p(IDT$_{C16}$-TPD$_{C8}$) compared to p(IDTT$_{C16}$-TPD$_{C8}$).

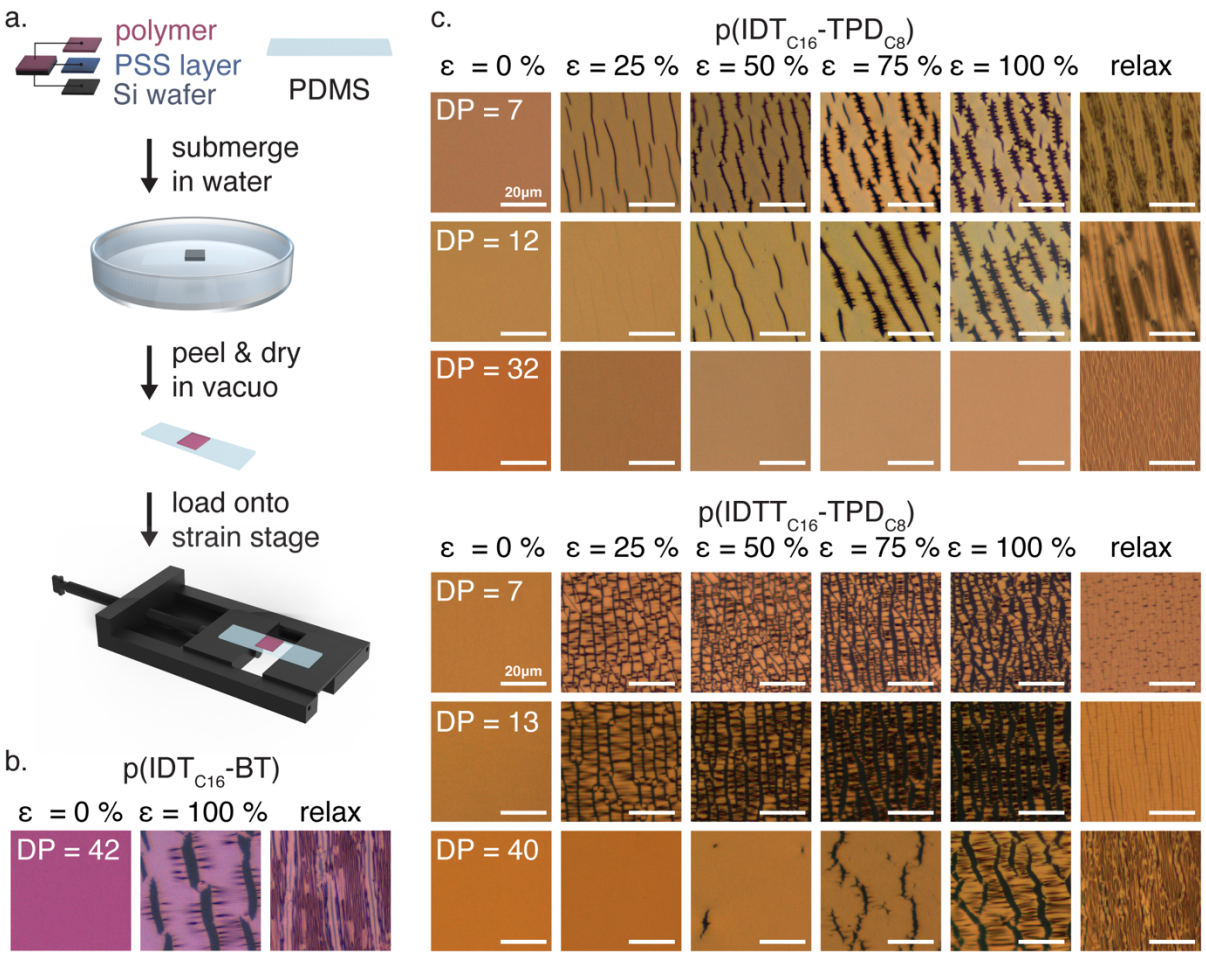

Figure 3. Mechanical properties characterization of thin films. a) The elastic modulus, *E*, was measured using a buckling-based metrology with a film-on-elastomer approach and the buckling wavelengths were extracted from optical microscopy. b) The samples for crack onset strain were prepared using a water-assisted film transfer onto PDMS and then loaded onto a homemade strain, c) where the formation of cracks was monitored by optical microscopy.

2.3. Photophysical characterization

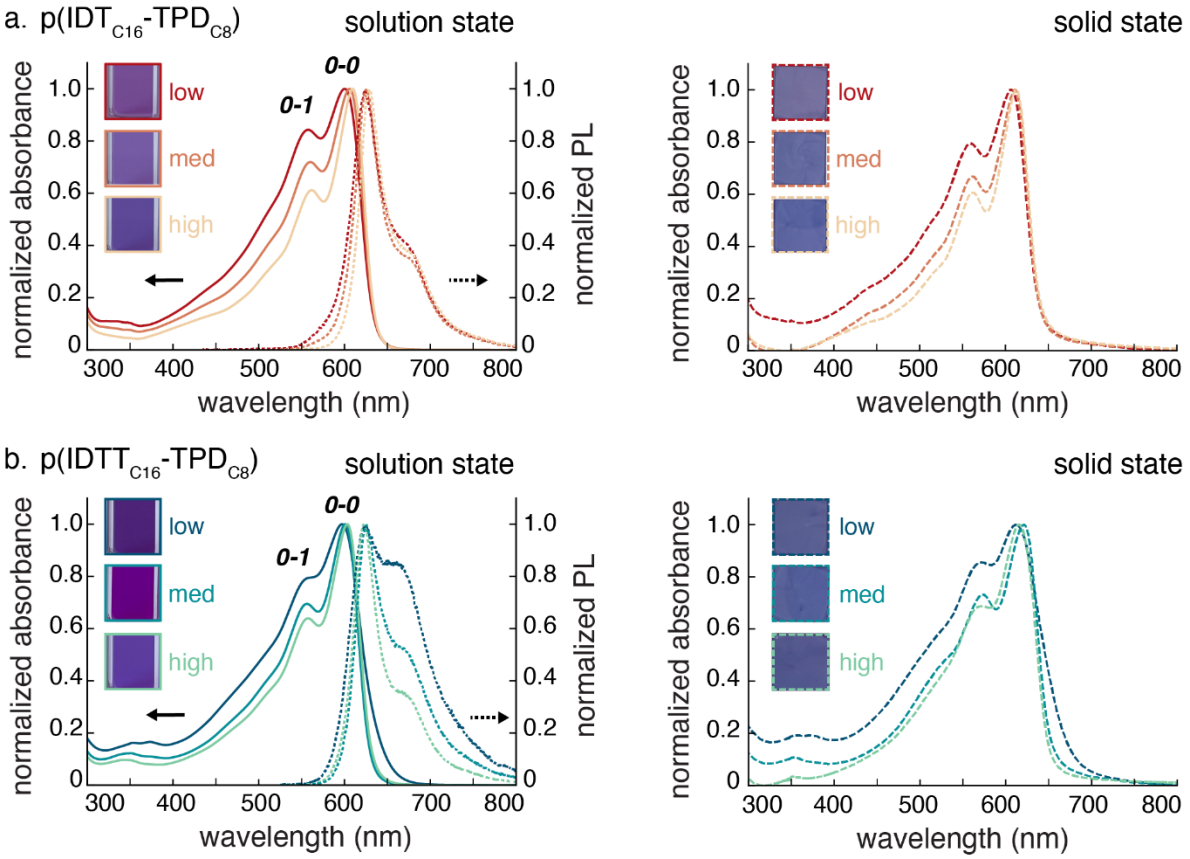

Figure 4. UV-vis absorption and PL spectra in solution-state and absorption spectra in solid-state (thin films) for a) p(IDT$_{C16}$-TPD $_{C8}$) and b) p(IDTT$_{C16}$-TPD$_{C8}$).

Ultraviolet–visible light absorption spectroscopy (UV–Vis) and photoluminescence (PL) experiments were performed to see the effect of MW and an extended donor unit on optical and aggregation properties. The absorption profile for both TPD-based copolymers primarily differs in the (0-0) transition (λ_{max}), which becomes more pronounced compared to the (0-1) transition (~540 nm) as MW increases. The $I_{0\text{-}0}/I_{0\text{-}1}$ ratio increases from 1.2 to 1.7 for p(IDT$_{C16}$-TPD$_{C8}$)-DP7 to -DP32 and 1.3 to 1.6 for p(IDTT$_{C16}$-TPD$_{C8}$)-DP7 to -DP40 (Table 2). The (0-0) transition is typically attributed to J-type polymer aggregation and so a higher $I_{0\text{-}0}/I_{0\text{-}1}$ ratio with increasing MW suggests increased J-type aggregation compared to H-type aggregation.[14,34–36] Additionally, as MW increases, λ_{max} exhibits a bathochromic shift by 8 nm from 601 nm for p(IDT$_{C16}$-TPD$_{C8}$)-DP7 to 609 nm for p(IDT$_{C16}$-TPD$_{C8}$)-DP32 (Figure 3a). This minimal bathochromic shift is also seen for p(IDTT$_{C16}$-TPD$_{C8}$), where λ_{max} red-shifts by 6 nm from 597 for p(IDTT$_{C16}$-TPD$_{C8}$)-DP7 to 603 nm for p(IDTT$_{C16}$-TPD$_{C8}$)-DP40

(Figure 3b). This bathochromic shift in λ_{max} as MW increases can be attributed to increasing chain length and the minimal difference indicates the high MW regime polymers in this study are approaching sufficiently high MW to achieve saturated optoelectronic properties.[37–40] The similarity in Stokes shift in solution-state between p(IDT_{C16}-TPD_{C8}) and p($IDTT_{C16}$-TPD_{C8}) across MWs contradicts what is expected as it suggests that the planarity and rigidity of the polymer backbone is not significantly altered by an extended donor unit. However, p($IDTT_{C16}$-TPD_{C8}) does exhibit a more pronounced red shift in λ_{max} upon casting into thin films from solution compared to p(IDT_{C16}-TPD_{C8}) by approximately triple (e.g., 13 nm for p($IDTT_{C16}$-TPD_{C8})-DP40 and 4 nm for p(IDT_{C16}-TPD_{C8})-DP32), suggesting the former adopts a higher degree of planarization in the solid state. This observation is as expected due to the increased conjugation length of the IDTT unit compared to IDT.

Table 2. Optoelectronic properties of TPD-based copolymers

	Solution-state				Solid-state	
Polymer	$\lambda_{max,abs}$ (nm)[a)]	$\lambda_{max,PL}$ (nm)[b)]	Stokes shift (nm)	$I_{0\text{-}0}/I_{0\text{-}1}$	$\lambda_{max,abs}$ (nm)[c)]	$\Delta_{sln\ to\ thin\ film,\ abs}$ (nm)
p(IDT_{C16}-TPD_{C8})	601	624	23	1.2	607	6
	606	625	19	1.4	611	5
	609	629	20	1.7	613	4
p($IDTT_{C16}$-TPD_{C8})	597	623	26	1.3	613	16
	601	622	21	1.4	621	20
	603	626	23	1.6	616	13

[a)] Measurements of solution state UV-Vis absorption and [b)] photoluminescence spectra were done in dilute chloroform. [c)]Measurements of solid-state UV-Vis absorption spectra were done on thin film samples prepared by spin coating polymer solutions onto glass slides.

2.4. Morphological and Electrical Characterization

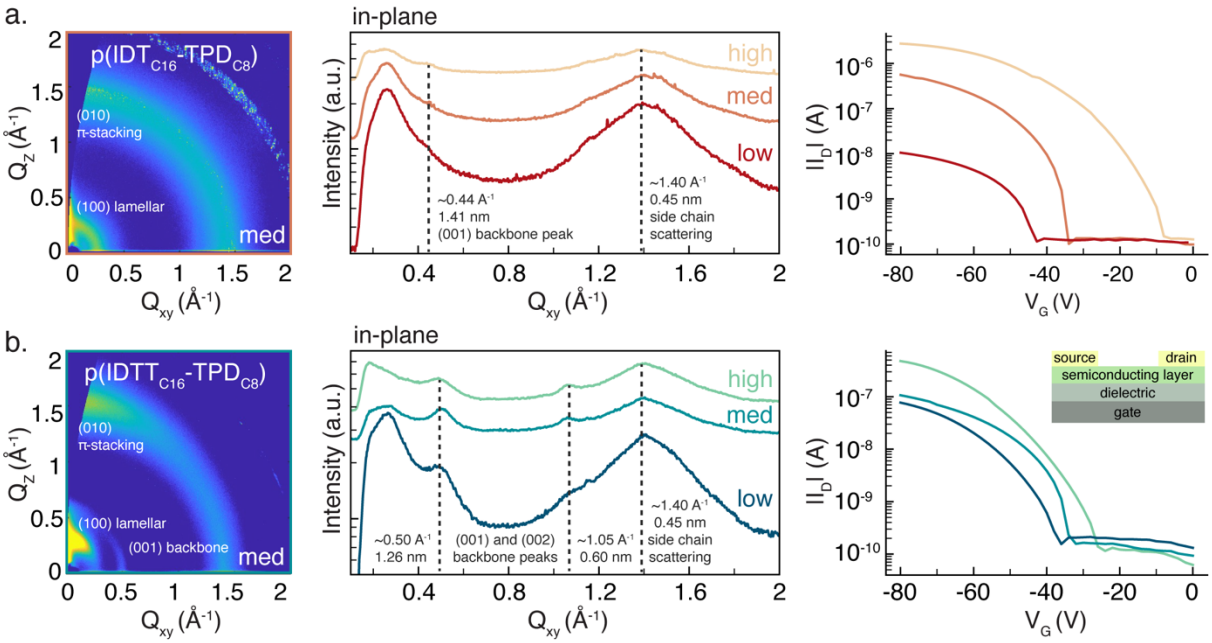

Figure 5. Morphological characterization of polymer thin films using GIWAXS. Representative 2D GIWAXS spectra for medium DP polymers of a) p(IDT$_{C16}$-TPD$_{C8}$) and b) p(IDTT$_{C16}$-TPD$_{C8}$) are shown. Linecuts of the 2D GIWAXS spectra in the Q_{xy} direction (in-plane) are shown as well with the (001) backbone peak labelled.

Impact of MW and extended core unit on morphology was analyzed by GIWAXS on as-cast thin-films of p(IDT$_{C16}$-TPD$_{C8}$) and p(IDTT$_{C16}$-TPD$_{C8}$). Relevant metrics are summarized in Table S4 and 2D spectra for all polymers can be found in the SI (S40). Both TPD-based copolymer series display broad out-of-plane π-stacking scattering peaks arising from (0k0) planes. In-plane π-stacking is difficult to deconvolute from the diffuse scatter apparent at Q_{xy} ~1.4 Å^{-1} for both series. This scatter has been attributed to scattering arising from the disordered alkyl side chains.[41] p(IDTT$_{C16}$-TPD$_{C8}$) shows π-stacking scattering peaks at Q_z = 1.54 Å^{-1} (D_π ~4.1 Å), matching closely with the reported π-stacking distance for p(IDT$_{C16}$-BT).[22,41] p(IDT$_{C16}$-TPD$_{C8}$) shows broad out-of-plane π-stacking scattering peaks at a reduced Q of Q_z ~1.42-1.45 Å^{-1} (D_π ~4.3-4.4 Å) in line with previous reports.[15] The π-stacking distance decreases slightly going from the low to the high DP in p(IDT$_{C16}$-TPD$_{C8}$). π-stacking structural coherence is low for both p(IDTT$_{C16}$-TPD$_{C8}$) and p(IDT$_{C16}$-TPD$_{C8}$) (~3-5 π-stacks), indicating little long-range interchain ordering. Lamellar structural coherence is

low as well for both TPD-based copolymer series. p(IDT_{C16}-TPD_{C8}) lamellar spacing (D_{lam} ~22-23 Å) is larger than that of p($IDTT_{C16}$-TPD_{C8}) (~20 Å), and both sets of material have smaller lamellar spacing than that of p(IDT_{C16}-BT)[19,22,41], possibly indicating less volume occupied by the side chains in p($IDTT_{C16}$-TPD_{C8}) and p(IDT_{C16}-TPD_{C8}). Interestingly, there is a broad shoulder at Q_z ~0.58 $Å^{-1}$ in p($IDTT_{C16}$-TPD_{C8}) that is most prominent in the medium molecular weight batch that possibly arises from a 2nd order lamellar feature, though this assignment is tentative.

For scattering from polymer backbone ordering along (00l) planes, p($IDTT_{C16}$-TPD_{C8}) across all DP (Figure 5b) displays strong in-plane scattering features at Q_{xy} ~0.50 $Å^{-1}$ and Q_{xy} ~1.05 $Å^{-1}$ ($D_{(001)}$ = 12.6 Å) whereas only p(IDT_{C16}-TPD_{C8})-DP32 (Figure 5a) shows a weak in-plane scattering feature at Q_{xy} = 0.44 $Å^{-1}$ ($D_{(001)}$ = 14.1 Å). Scattering arising from backbone ordering requires some degree of *inter*chain registry, and thus does not necessarily arise from scattering features that correspond precisely to monomer-monomer repeat distances. The assignment of exact physical features to the backbone scattering is highly dependent on how polymer chains are aligned relative to each other.[22,42] Given the larger monomer units of p($IDTT_{C16}$-TPD_{C8}) compared to p(IDT_{C16}-TPD_{C8}) but *shorter* backbone scattering feature of $D_{(001)}$ = 12.6 Å for p($IDTT_{C16}$-TPD_{C8}) compared to $D_{(001)}$ = 14.1 Å for p(IDT_{C16}-TPD_{C8}), it is a reasonable hypothesis that p($IDTT_{C16}$-TPD_{C8}) might have preferential interchain crossing angles that are more shallow than those of p(IDT_{C16}-TPD_{C8}), though this is speculative. We also previously hypothesized that the presence of the (001) signal could indicate side chain interdigitation, where the alkyl chains interdigitate and cause the polymer chains to pack closely, allowing for translational order between chains and increased electrical performance.[15] In agreement with this hypothesis, p(IDT_{C16}-TPD_{C8}) was previously observed to lack the (001) backbone scattering feature and showed a decrease in mobility compared to other CPs tested that did possess the (001) feature. The lack of sidechain interdigitation in p(IDT_{C16}-TPD_{C8}) was thought to be potentially caused by the long octyl sidechain of the

TPD_{C8} monomer requiring more space to interdigitate. Therefore, we hypothesized that the use of an extended donor unit, such as IDTT, could provide extra space for the alkyl chains to pack, enabling sidechain interdigitation and improving electrical performance. This hypothesis is supported by the findings in this study where scattering from polymer backbone ordering along (00l) planes is seen in p($IDTT_{C16}$-TPD_{C8}) across all DP but still not seen in p(IDT_{C16}-TPD_{C8}) in the low and medium DP and only weakly with the high DP.

To study the impact of the extended core on charge carrier mobility, bottom-gate top-contact organic field effect transistors (OFETs) were fabricated using both p(IDT_{C16}-TPD_{C8}) and p($IDTT_{C16}$-TPD_{C8}) (Figure 5). The operating characteristics of these devices are summarized in Table S5 in the SI. For p(IDT_{C16}-TPD_{C8}), average μ_{hole} increases from 0.044 $\pm$ 0.026 x 10^{-3} $cm^2V^{-1}s^{-1}$ for p(IDT_{C16}-TPD_{C8})-DP7, 1.5 $\pm$ 0.63 x 10^{-3} $cm^2V^{-1}s^{-1}$ for p(IDT_{C16}-TPD_{C8})-DP12, to 7.4 $\pm$ 1.9 x 10^{-3} $cm^2V^{-1}s^{-1}$ for p(IDT_{C16}-TPD_{C8})-DP32. Based on the UV-Vis observations and the strong in-plane scattering features attributed to polymer backbone ordering along (001) planes from GIWAXS, charge-carrier mobilities for the p($IDTT_{C16}$-TPD_{C8}) series were expected to be the same or higher compared to the p(IDT_{C16}-TPD_{C8}) series. However, average μ_{hole} for p($IDTT_{C16}$-TPD_{C8}) was lower for both p($IDTT_{C16}$-TPD_{C8})-DP13 (0.41 $\pm$ 0.06 x 10^{-3} $cm^2V^{-1}s^{-1}$) and p($IDTT_{C16}$-TPD_{C8})-DP40 (2.0 $\pm$ 0.36 x 10^{-3} $cm^2V^{-1}s^{-1}$) when compared to their p(IDT_{C16}-TPD_{C8}) counterpart. Only the low DP polymers followed the hypothesized trend with the average μ_{hole} for (p($IDTT_{C16}$-TPD_{C8})-DP7 being 0.30 $\pm$ 0.14 $cm^2V^{-1}s^{-1}$ and p(IDT_{C16}-TPD_{C8})-DP7 being 0.044 $\pm$ 0.026 x 10^{-3} $cm^2V^{-1}s^{-1}$. These polymers are 1-dimensional (1D) transporters with occasional interchain crosses that facilitate chain-to-chain charge hopping.[43,44] For the IDT-based series, the higher DP likely facilitates more 1D transport but also increases the number of interchain crosses, resulting in higher average μ_{hole}. For the IDTT-based series, the greater crystallinity implies more regions of parallel chains (i.e., less of the individual chains crossing). Hence the observed lower mobility and less change with increase in DP. While these are hypotheses and more investigation is needed, our

study points towards unique charge transport properties of IDT-based polymers. <Need more hypotheses> Overall, the morphological thin film observations show that the p(IDT_{C16}-TPD_{C8}) series does have more interchain crosses (i.e., more entanglements) with greater DP, which can explain the higher CoS observed. The charge mobility trend in IDTT suggests that the entanglement and/or interchain crosses do not increase with DP so less of an increase is observed with CoS for the p($IDTT_{C16}$-TPD_{C8}) series with higher DP.

3. Conclusion

In summary, we demonstrated that increasing DP of p(IDT_{C16}-TPD_{C8}) significantly improves stretchability (*CoS* from *ca.* 2 to 100%) while maintaining an *E* in the 10s of MPa range (13 to 32 MPa) and increasing average μ_{hole}. When optimizing reaction conditions for DArP, the introduction of a diamine co-ligand (TMEDA) can appreciably improve yield and DP. Using stoichiometric ratios to control the DP of CPs was a viable approach for p(IDT_{C16}-TPD_{C8}) but proved difficult to replicate with p($IDTT_{C16}$-TPD_{C8}), highlighting the importance of optimizing reaction conditions for each copolymer when using DArP. Extending the π-conjugation of the IDT unit to IDTT did not result in greater average μ_{hole} when comparing medium and high DP p($IDTT_{C16}$-TPD_{C8}) to its p(IDT_{C16}-TPD_{C8}) counterparts despite their higher crystallinity and (001) peak observed by GIWAXS. Further investigation to elucidate the differences in structural order of these TPD-based copolymers could help explain the observed trends. Exploration of other extended core IDT units could also improve electrical performance of (IDT_{C16}-TPD_{C8}).

4. Experimental Section

Representative polymerization procedure, p(IDT_{C16}-TPD_{C8}): In a glovebox, a mixture of IDT_{C16} (90 mg, 0.08 mmol), TPD_{C8}-Br_2 (37.9 mg, 0.08 mmol), tris(dibenzylideneacetone)dipalladium(0) (3.5 mg, 5 mol%), tris(o-anisyl)phosphine (2.7 mg, 10 mol%), cesium carbonate (125 mg, 0.38 mmol) and pivalic acid (3.9 mg, 0.025 mmol) in a 4 mL vial was added anhydrous o-xylene (1 mL). The vial was sealed with a PTFE lined cap and the mixture was pre-stirred at room temperature for 2 minutes to get a homogenous mixture before heating to 100 °C for 16 h, followed by being cooled to room temperature and

precipitation into methanol (100 mL). The precipitate was filtered through a Soxhlet thimble and then purified by Soxhlet extraction with methanol, acetone, and hexanes. The hexanes fraction was collected, and the solvent was removed by rotary evaporation. The residue was dissolved in chloroform and precipitated into methanol. The precipitate was collected by filtration and dried under vacuum to afford a deep purple solid. Detailed characterization in SI (NMR spectroscopy, Figure S21-S39).

Thin Film Preparation: Bare Si wafers were cleaned with acetone, methanol, and DI water and then dried under vacuum before being plasma treated (ambient air, 150 mTorr, 3 minutes; PE-50 Plasma Etcher). The substrates were then spin cast with 3 wt % PSS (aq. DI water, 120 uL) at 4000 rpm for 60 seconds and annealed at 80°C for ~10 seconds to drive off remaining water. Polymer solutions were prepared by dissolving in anhydrous chloroform at a 10 mg/mL concentration and stirred on a hot plate with a magnetic stirrer at 50°C for 2-4 hours before filtering through a 0.22 μm PTFE filter. Filtered polymer solutions were spin cast onto the Si wafers (drop on and then spin coat, not annealed) at 1500 rpm for 60 seconds.

Mechanical Characterizations, Film-on-Elastomer Preparation: PDMS (Sylgard 184, Dow Corning) was prepared by vigorously mixing the base resin and the curing agent in 20:1 (by weight) ratio, pouring into a Petri dish, and leaving under dynamic vacuum at ambient temperature for 2 hours before curing at 65 °C for 12 h in an oven. The PDMS strips were then cut (4 cm x 1 cm x 0.5 cm) with a scalpel. 10:1 PDMS was also tested for samples (Figure S4-S5) to see the effect of the elastomeric substrate on crack behavior. The same trend with increasing MW leading to increasing *CoS* was observed for 10:1, except the *CoS* values were higher for 10:1 compared to 20:1. 20:1 PDMS (0.65 MPa) was selected as the primary elastomeric substrate as it shows the trend more drastically than 10:1 (2.2 MPa). The elastic modulus of PDMS was measured using a CellScale Univert S Mechanical Test System (4.5 N load cell) and obtained from the slope of the linear fit of the stress-strain curve in the elastic region (cut to ISO 37 – Type 4 standard).

Mechanical Characterizations, Film-on-Elastomer CoS: For crack onset strain measurements, the polymer thin films were transferred to the PDMS by pressing the Si wafer onto the PDMS strip and then submerging it into a DI water bath. After 5-30 minutes (depending on sample), the PDMS sample was removed from the water bath and the Si wafer was carefully removed with tweezers to give the thin film polymer on the PDMS. The sample was dried in a

desiccator under dynamic vacuum for 2 hours before loading onto a homemade strain stage. The formation of cracks was observed using an optical microscope (Zeiss Axio Imager.A2m) incrementally from 0 to 100 % strain to relaxation.

Mechanical Characterizations, Film-on-Elastomer Buckling Method: The same protocol for *CoS* film transfer was followed except the PDMS (20:1) was pre-strained to 2% strain before transferring the polymer thin film. After removing from the DI water bath, the Si wafer was carefully removed, and the sample dried under dynamic vacuum in a desiccator for ~2 hours before releasing the strain. The strain was removed right before imaging to avoid potential stress-relaxation and/or reduction in amplitude of the buckles. The thickness of each polymer film (d_f) was measured using AFM (Bruker, Nanoscope). The average elastic modulus of the thin film (E_f) was calculated from the equation below:

$$E_f = 3E_s\left(\frac{1-v_f^2}{1-v_s^2}\right)\left(\frac{\lambda_b}{2\pi d_f}\right)^3$$

Where E_s is the elastic modulus for the substrate (PDMS), v_f and v_s are the Poisson ratios of the film and PDMS substrate respectively (assumed to be 0.35 and 0.5), d_f is the film thickness, and $\lambda_b$is the buckling wavelength. λ_b is based on counting the number of buckles in a row in a length and then dividing that length by the number of buckles counted. This was done five times across at least 2 different optical microscopy images (Zeiss Axio Imager.A2m; Figure S6) to get 5 values for λ_b. E_f was calculated using each λ_b and averaged to get average E_f.

Mechanical Characterizations, Film-on-Water: Tensile tests of conjugated polymer thin films were performed by tensile draw for films floating on water surface. The films were prepared on spin coating on the top of PSS- coated Si wafers followed by being floated on top of water and stretched at a strain rate of 0.005 s^{-1} until fracture. The detailed instrument setup can be found in previous literature reports.

Optoelectronic Measurements: UV-vis absorption spectra were measured on Agilent Cary 7000 UV-Vis-NIR Universal Measurement spectrophotometer (spectral range 170 - 3000 nm, double beam instrument) and a 100% transmittance sample was recorded as a blank using chloroform in a quartz cuvette. PL spectra were measured on a Horiba Fluorolog-3 spectrofluorometer with an excitation wavelength of 420 nm and emission spectra collected from 500 to 800 nm. Solution measurements were performed in chloroform solutions

(polymer concentration: p(IDT-BT) and p(IDTT-TPD $_{C8}$), 0.02 mgmL^{-1}; p(IDT-TPD$_{C8}$), 0.06 mgmL^{-1}). Thin films used for solid-state absorption measurements were spin cast from a chloroform solution with a polymer concentration of 5 mgmL^{-1} onto 5 by 5 mm glass substrates.

Crystallographic Measurements: Samples for GIWAXS measurements were prepared by spin-coating 5 mgmL^{-1} polymer solutions in $CHCl_3$ onto lightly doped n-type silicon substrates with a native oxide layer. Polymer solutions were stirred at 55°C overnight and filtered with 0.45-micron PVDF filters prior to spin-coating. Spin-coating was performed at 1500 rpm for 60 seconds, yielding films of ~50-60 nm thick. All sample preparation was performed in a nitrogen glovebox (O_2 < 0.5 ppm). GIWAXS measurements were performed at Stanford Synchrotron Radiation Lightsource, SLAC National Accelerator Laboratory, Beamline 11-3. A flat area detector (Rayonix MAR-225) was used. The X-ray incident energy was 12.7 keV and an incident angle of 0.1° was used. GIWAXS data was corrected for geometric distortions imposed by the flat area detector and reduced/analyzed using a combination of Nika 1D SAXS and WAXStools software packages in Igor Pro.[45,46] All data is reported in terms of the scattering vector, Q where $Q = 4\pi \sin(\theta)/\lambda$ where θ is the scattering half angle and λ is the incident X-ray wavelength. All GIWAXS measurements were performed in a helium purged chamber to minimize X-ray air scatter and sample beam damage.

Electrical Characterizations: Heavily boron-doped silicon substrates with a 300 nm (± 5 nm) thick thermal oxide layer (University Wafer) as a gate dielectric were used for the thin-film field-effect transistors (FETs). Substrates were first scrubbed with detergent and water and then sonicated in DI water, acetone, and isopropyl alcohol for 15 min per solvent, followed by drying under a stream of compressed nitrogen. To passivate the thermal oxide, a self-assembled monolayer of octadecyl trimethoxy silane (OTMS) was deposited on the cleaned substrates using a literature technique with slight modifications.[3] The substrates were cleaned in a plasma cleaner for 15 min using air plasma. They were then quickly spin coated with a solution of 3 mM OTMS in trichloroethylene. The substrates were placed in a chamber that was being fed nitrogen through a bubbler with saturated ammonium hydroxide into the chamber overnight at room temperature and ambient pressure. The substrates were rinsed with toluene and then isopropyl alcohol for 5 minutes each to remove any physiosorbed ODTS from the surface, followed by drying under a stream of compressed nitrogen. Polymer

solutions were stirred at 55°C overnight and filtered with 0.45-micron PVDF filters prior to spin-coating. The polymer layer was then spin-coated from a 5 or 10 mg/mL solution of each polymer in $CHCl_3$ at 2000 RPM for 60 s onto the OTMS passivated substrates in a nitrogen environment. Gold electrodes were thermally evaporated onto the active layer to a thickness of 100 nm at a rate of 0.5 Å s^{-1}. The gold was evaporated from an alumina coated molybdenum boat and the electrodes were deposited through a shadow mask. After electrode deposition, the devices were tested for charge mobility, threshold voltage and current on/off ratio. The devices had a top-contact bottom-gate architecture with a channel width of 1000 µm and a channel length of 50 µm. They were tested in a nitrogen atmosphere using an Everbeing Int'l Corp C-2 Mini Station and a Keithley Model 4200A-SCS Parameter Analyzer. The transfer curves were collected in the saturation regime, where the linear section of the curve was fitted to estimate the charge mobility using the following equation:

$$I_D = \frac{WC\mu}{2L}(V_G - V_T)^2$$

where I_D is the drain-source current; µ is the charge mobility; W is the channel width; L is the channel length; C is the capacitance per unit area of the insulator (SiO_2, 300 nm, 10 nF·cm^{-2}). V_G is the gate voltage; and V_T is the threshold voltage. The threshold voltage was obtained by fitting the linear region of the ${I_D}^{1/2}$vs V_G curve and extrapolating to $I_D = 0$. Measurements were averaged from at least three devices across two chips.

Data Visualization Code: Python scripts created in lab were used to calculate μ_{avg}, I_{on}/I_{off}, and V_{th} as well as to plot all transfer and output curves. The code repository can be found at https://github.com/teamtran/data-visualizer/tree/v0.1.0-alpha-ofet. The relevant Python scripts are found under the "Electrical" directories (https://github.com/teamtran/data-visualizer/tree/v0.1.0-alpha-ofet/code/Electrical, https://github.com/teamtran/data-visualizer/tree/v0.1.0-alpha-ofet/scripts/Electrical).

Supporting Information

Supporting Information is available from the Wiley Online Library or from the author.

Conflict of Interest

The authors declare no conflict of interest.

Acknowledgements

This work was supported in part by the Mitacs-JSPS summer program, the Natural Sciences and Engineering Research Council (NSERC) of Canada (H.T., RGPIN2021-03554; A.L., S.L. major scholarship), the Canadian Foundation for Innovation (H.T.: JELF-41743), the U.S. Department of Energy (DOE), Office of Science, Basic Energy Sciences (BES), under award DE-SC0020046 (L.G.), and JSPS KAKENHI Grant Number JP24K08518. This research was undertaken also thanks in part to funding provided to the University of Toronto's Acceleration Consortium from the Canada First Research Excellence Fund. Part of this work was conducted at the UW Photonics Center and Research Training Testbeds supported by the Clean Energy Institute and the Molecular Analysis Facility, a National Nanotechnology Coordinated Infrastructure site at the University of Washington which is supported in part by the National Science Foundation (grant NNCI-1542101), the University of Washington, the Molecular Engineering & Sciences Institute, and the Clean Energy Institute. Support by the Okinawa Institute of Science and Technology is also acknowledged. Y.W. and X.G. thanks the financial aid from NSF grant DMR-2047689 for supporting thin film mechanical characterization technique used in this work.

Contributions

A.L. conceptualization (lead), data curation (lead), formal analysis (lead), writing (lead); G.L. GIWAXS data curation and analysis (lead), writing-review & editing (supporting); L.G. OFET data curation (supporting), formal analysis (supporting), writing-review & editing (supporting); S.L. OFET python script creation (lead), data curation (supporting), formal analysis (supporting), writing-review & editing (supporting), figure creation (supporting); A.S. tensile tester creation (lead), writing-review & editing (supporting); Y.W. FOW data curation (lead), writing-review & editing (supporting); Xiaodan Gu data curation (supporting), investigation (supporting), supervision (supporting), writing-review & editing (supporting); Alberto Salleo data curation (supporting), supervision (supporting), writing-review & editing (supporting); Christine K. Luscombe conceptualization (lead), formal analysis (colead), funding acquisition (colead), project administration (colead), supervision (colead), writing-review & editing (colead); Helen Tran conceptualization (supporting),

formal analysis (colead), funding acquisition (colead), project administration (colead), supervision (colead), writing-review & editing (colead).

Received: ((will be filled in by the editorial staff))
Revised: ((will be filled in by the editorial staff))
Published online: ((will be filled in by the editorial staff))

References

[1] J. Xu, H. C. Wu, C. Zhu, A. Ehrlich, L. Shaw, M. Nikolka, S. Wang, F. Molina-Lopez, X. Gu, S. Luo, D. Zhou, Y. H. Kim, G. J. N. Wang, K. Gu, V. R. Feig, S. Chen, Y. Kim, T. Katsumata, Y. Q. Zheng, H. Yan, J. W. Chung, J. Lopez, B. Murmann, Z. Bao, *Nat Mater* **2019**, *18*, 594.
[2] G.-J. Nathan Wang, A. Gasperini, Z. Bao, G. N. Wang, A. Gasperini, Z. Bao, *Adv Electron Mater* **2018**, *4*, 1700429.
[3] C. Zhao, J. Park, S. E. Root, Z. Bao, *Nat. Rev. Bioeng.* **2024**, *2*, 671.
[4] N. Matsuhisa, D. Inoue, P. Zalar, H. Jin, Y. Matsuba, A. Itoh, T. Yokota, D. Hashizume, T. Someya, *Nat Mater* **2017**, *16*, 834.
[5] J. Xu, S. Wang, G. J. N. Wang, C. Zhu, S. Luo, L. Jin, X. Gu, S. Chen, V. R. Feig, J. W. F. To, S. Rondeau-Gagné, J. Park, B. C. Schroeder, C. Lu, J. Y. Oh, Y. Wang, Y. H. Kim, H. Yan, R. Sinclair, D. Zhou, G. Xue, B. Murmann, C. Linder, W. Cai, J. B. H. Tok, J. W. Chung, Z. Bao, *Science* **2017**, *355*.
[6] A. Gasperini, S. Bivaud, K. Sivula, *Chem Sci* **2014**, *5*, 4922.
[7] Y. Zhao, X. Zhao, Y. Zang, C. A. Di, Y. Diao, J. Mei, *Macromolecules* **2015**, *48*, 2048.
[8] A. Gasperini, G. J. N. Wang, F. Molina-Lopez, H. C. Wu, J. Lopez, J. Xu, S. Luo, D. Zhou, G. Xue, J. B. H. Tok, Z. Bao, *Macromolecules* **2019**, *52*, 2476.
[9] N. S. Y. Hsu, A. Lin, H. Tran, *Acc Mater Res* **2023**, *4*, 205.
[10] S. P. Lacour, G. Courtine, J. Guck, *Nat Rev Mater* **2016**, *1*, 16063.
[11] X. Zhou, Y. Wang, J. Ji, P. Zhang, *Adv. Healthcare Mater.* **2024**, *13*, 2304478.
[12] S. Capuani, G. Malgir, C. Y. X. Chua, A. Grattoni, *Bioeng Transl Med* **2022**, *7*, e10300.
[13] B. Zhao, D. Pei, Y. Jiang, Z. Wang, C. An, Y. Deng, Z. Ma, Y. Han, Y. Geng, *Macromolecules* **2021**, *54*, 9896.

[14] Y. Li, W. K. Tatum, J. W. Onorato, Y. Zhang, C. K. Luscombe, *Macromolecules* **2018**, *51*, 6352.
[15] P. J. W. Sommerville, A. H. Balzer, G. Lecroy, L. Guio, Y. Wang, J. W. Onorato, N. A. Kukhta, X. Gu, A. Salleo, N. Stingelin, C. K. Luscombe, *ACS Polym. Au* **2023**, *3*, 59.
[16] D. Rodriquez, J. H. Kim, S. E. Root, Z. Fei, P. Boufflet, M. Heeney, T. S. Kim, D. J. Lipomi, *ACS Appl Mater Interfaces* **2017**, *9*, 8855.
[17] D.-C. Kong, M.-H. Yang, X.-S. Zhang, Z.-C. Du, Q. Fu, X.-Q. Gao, J.-W. Gong, *Macromol. Mater. Eng.* **2021**, *306*, 2100536.
[18] F. P. V. Koch, J. Rivnay, S. Foster, C. Müller, J. M. Downing, E. Buchaca-Domingo, P. Westacott, L. Yu, M. Yuan, M. Baklar, Z. Fei, C. Luscombe, M. A. McLachlan, M. Heeney, G. Rumbles, C. Silva, A. Salleo, J. Nelson, P. Smith, N. Stingelin, *Prog. Polym. Sci.* **2013**, *38*, 1978.
[19] J. F. Ponder, H. Chen, A. M. T. Luci, S. Moro, M. Turano, A. L. Hobson, G. S. Collier, L. M. A. Perdigão, M. Moser, W. Zhang, G. Costantini, J. R. Reynolds, I. McCulloch, *ACS Mater Lett* **2021**, *3*, 1503.
[20] W. Zhang, Y. Han, X. Zhu, Z. Fei, Y. Feng, N. D. Treat, H. Faber, N. Stingelin, I. McCulloch, T. D. Anthopoulos, M. Heeney, *Adv. Mater.* **2016**, *28*, 3922.
[21] A. Wadsworth, H. Chen, K. J. Thorley, C. Cendra, M. Nikolka, H. Bristow, M. Moser, A. Salleo, T. D. Anthopoulos, H. Sirringhaus, I. McCulloch, *J Am Chem Soc* **2020**, *142*, 652.
[22] C. Cendra, L. Balhorn, W. Zhang, K. O'Hara, K. Bruening, C. J. Tassone, H.-G. Steinrück, M. Liang, M. F. Toney, I. McCulloch, M. L. Chabinyc, A. Salleo, C. J. Takacs, *ACS Macro Lett.* **2021**, *10*, 1306.
[23] R. M. W. Wolfe, J. R. Reynolds, *Org Lett* **2017**, *19*, 996.
[24] J. F. Ponder, H. Chen, A. M. T. Luci, S. Moro, M. Turano, A. L. Hobson, G. S. Collier, L. M. A. Perdigão, M. Moser, W. Zhang, G. Costantini, J. R. Reynolds, I. McCulloch, *ACS Mater Lett* **2021**, *3*, 1503.
[25] E. Iizuka, M. Wakioka, F. Ozawa, *Macromolecules* **2016**, *49*, 3310.
[26] G. L. Gibson, D. Gao, A. A. Jahnke, J. Sun, A. J. Tilley, D. S. Seferos, *J Mater Chem A Mater* **2014**, *2*, 14468.
[27] W. Li, L. Yang, J. R. Tumbleston, L. Yan, H. Ade, W. You, *Adv. Mater.* **2014**, *26*, 4456.
[28] D. Tank, H. H. Lee, D. Y. Khang, *Macromolecules* **2009**, *42*, 7079.
[29] B. Wang, S. Bao, S. Vinnikova, P. Ghanta, S. Wang, *npj flex. electron.* **2017**, *1*, 5.
[30] J. Y. Chung, A. J. Nolte, C. M. Stafford, *Adv. Mater.* **2011**, *23*, 349.
[31] C. M. Stafford, C. Harrison, K. L. Beers, A. Karim, E. J. Amis, M. R. Vanlandingham, H. C. Kim, W. Volksen, R. D. Miller, E. E. Simonyi, *Nat Mater* **2004**, *3*, 545.
[32] B. O'Connor, E. P. Chan, C. Chan, B. R. Conrad, L. J. Richter, R. J. Kline, M. Heeney, I. McCulloch, C. L. Soles, D. M. DeLongchamp, *ACS Nano* **2010**, *4*, 7538.
[33] B. Roth, S. Savagatrup, N. V. De Los Santos, O. Hagemann, J. E. Carlé, M. Helgesen, F. Livi, E. Bundgaard, R. R. Søndergaard, F. C. Krebs, D. J. Lipomi, *Chem. Mater.* **2016**, *28*, 2363.
[34] P. J. W. Sommerville, Y. Li, B. X. Dong, Y. Zhang, J. W. Onorato, W. K. Tatum, A. H. Balzer, N. Stingelin, S. N. Patel, P. F. Nealey, C. K. Luscombe, *Macromolecules* **2020**, *53*, 7511.
[35] X. Yu, L. Chen, C. Li, C. Gao, X. Xue, X. Zhang, G. Zhang, D. Zhang, *Adv. Mater.* **2023**, *35*, 2209896.
[36] D. Liu, J. Mun, G. Chen, N. J. Schuster, W. Wang, Y. Zheng, S. Nikzad, J. C. Lai, Y. Wu, D. Zhong, Y. Lin, Y. Lei, Y. Chen, S. Gam, J. W. Chung, Y. Yun, J. B. H. Tok, Z. Bao, *J Am Chem Soc* **2021**, *143*, 11679.

[37] D. Adamczak, A. Perinot, H. Komber, A. Illy, S. Hultmark, B. Passarella, W. L. Tan, S. Hutsch, D. Becker-Koch, C. Rapley, A. D. Scaccabarozzi, M. Heeney, Y. Vaynzof, F. Ortmann, C. R. McNeill, C. Müller, M. Caironi, M. Sommer, *J. Mater. Chem. C,* **2021**, *9*, 4597.
[38] L. Zhang, N. S. Colella, F. Liu, S. Trahan, J. K. Baral, H. H. Winter, S. C. B. Mannsfeld, A. L. Briseno, *J. Am. Chem. Soc* **2013**, *135*, 844.
[39] H. Meier, *Angew. Chem. Int. Ed* **2005**, *44*, 2482.
[40] J. Lawrence, E. Goto, J. M. Ren, B. Mcdearmon, D. S. Kim, Y. Ochiai, P. G. Clark, D. Laitar, T. Higashihara, C. J. Hawker, *J. Am. Chem. Soc* **2017**, *139*, 13735.
[41] X. Zhang, H. Bronstein, A. J. Kronemeijer, J. Smith, Y. Kim, R. J. Kline, L. J. Richter, T. D. Anthopoulos, H. Sirringhaus, K. Song, M. Heeney, W. Zhang, I. McCulloch, D. M. Delongchamp, *Nat Commun* **2013**, *4*, 2238.
[42] H. Makki, C. A. Burke, A. Troisi, *J. Phys. Chem. Lett.* **2023**, *14*, 8867.
[43] G. LeCroy, R. Ghosh, P. Sommerville, C. Burke, H. Makki, K. Rozylowicz, C. Cheng, M. Weber, W. Khelifi, N. Stingelin, A. Troisi, C. Luscombe, F. C. Spano, A. Salleo, *J Am Chem Soc* **2024**, *146*, 21778.
[44] J. F. Coker, S. Moro, A. S. Gertsen, X. Shi, D. Pearce, M. P. van der Schelling, Y. Xu, W. Zhang, J. W. Andreasen, C. R. Snyder, L. J. Richter, M. J. Bird, I. McCulloch, G. Costantini, J. M. Frost, J. Nelson, *PNAS* **2024**, *121*, e2403879121.
[45] J. Ilavsky, *J Appl Crystallogr* **2012**, *45*, 324.
[46] S. D. Oosterhout, V. Savikhin, J. Zhang, Y. Zhang, M. A. Burgers, S. R. Marder, G. C. Bazan, M. F. Toney, *Chem. Mater.* **2017**, *29*, 3062.

ToC figure